2024 NDIA MICHIGAN CHAPTER
GROUND VEHICLE SYSTEMS ENGINEERING
AND TECHNOLOGY SYMPOSIUM
MODELING, SIMULATION, PROTOTYPING & VALIDATION (MSPV) TECHNICAL SESSION
AUGUST 13-15, 2024 - NOVI, MICHIGAN

Assessment of Artificial Magnetic Conductor Checkerboard-Arranged Applique for Ground System Radar Cross Section Reduction

Nathan Tison, PhD[1], Jeffrey D'Archangel, PhD[1]

[1] US Army DEVCOM GVSC, Warren, MI

ABSTRACT

A potentially effective means for ground system radar cross section reduction (RCSR) involves a checkerboard-arranged applique (ACA) composed of artificial magnetic conductor (AMC) metasurfaces which can result in phase modification – and thus destructive interference – of the reflected radar energy. This effort focused on the development of such a concept through the following main tasks: (1) the development of performance goals; (2) the selection of the AMC topology pattern; (3) the development of various performance models based upon transmission line theory and antenna planar array theory, and the use of various computational electromagnetics (CEM) solvers; (4) model validation; (5) the optimization of the AMC pattern through a design of experiment (DOE) approach; and (6) the development of a genetic programming framework for more rigorous ACA optimization.

Citation: N. Tison, J. D'Archangel, "Assessment of Artificial Magnetic Conductor Checkerboard-Arranged Applique for Ground System Radar Cross Section Reduction," In *Proceedings of the Ground Vehicle Systems Engineering and Technology Symposium* (GVSETS), NDIA, Novi, MI, Aug. 13-15, 2024.

1. INTRODUCTION

1.1. Background and Motivation

Simply put, radar cross section (RCS) is basically a measure of materiel detectability by threat radar, and is therefore something we would generally want to reduce. An advantageous means of RCS reduction (RCSR) would involve: (1) redirecting the reflected radar energy away from the receiver; (2) broadband performance; (3) no significant change to the materiel geometry; (4) the use of only a thin / light structure / applique; and (5) passive operation. One potential way to accomplish all of these goals would involve the use of a two-dimensional metamaterial (or metasurface).

A type of metasurface which can be used could consist of artificial magnetic conductors (AMCs) composed of a ground plane, a dielectric substrate, and a metallic patch pattern; see Fig. 1. The benefit of these AMCs is that they involve reflection phases which vary "continuously from +180° to -180° as the frequency increases" [1] through some resonant condition. Two different AMCs could be selected and configured in a square checkerboard pattern for purposes of maximizing the destructive interference of the radar energy reflected in the specular direction over as broad a bandwidth as possible, with the single, large, specular reflection lobe being exchanged for four, small, non-specular reflection lobes [3]. A relatively thin AMC checkerboard-arranged applique (ACA) could be constructed and adhered to materiel surfaces for RCSR purposes.

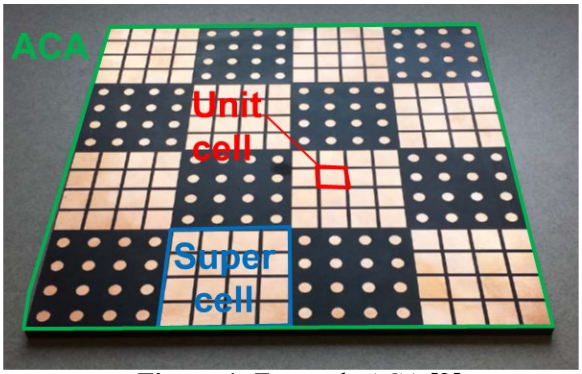

Figure 1: Example ACA [3].

1.2. Objectives

For the first year, the main goals of this study included: (1) the development of an efficient methodology for identifying / designing an ACA concept which satisfies RCSR performance requirements and other constraints; (2) the development of both simpler lumped-parameter models (LPM) and more computationally-intensive high-fidelity models (HFM) of ACA concept performance, and model validation using literature data; and (3) the general performance assessment of the most promising ACA concept, including RCS assessment of a PEC plate with and without the integrated ACA concept using a medium-fidelity model (MFM), which would also be validated.

For the second year, the objective is the development of an automated genetic programming (GP) approach for ACA concept synthesis and optimization.

1.3. Requirement Development

In order to have a standard against which the performance of the developed ACA concepts could be assessed, a set of performance goals was developed. Along these lines the following requirement verbiage was developed: "The applique should provide an average RCSR relative to a perfect electrical conductor (PEC) surface – from L- to X-band, for both transverse electric field (TE) and transverse magnetic field (TM) polarizations, and for normal incidence – which is greater than 10dB over at least 50% of the bandwidth, and is characterized by a bandwidth-averaged return elevation angle delta (with respect to normal incidence) which is as close to 45 degrees as possible."

As can be noted the goals, the following performance metrics can be identified: (1) the frequency-averaged RCSR or metric #1, to be minimized; (2) the under-10dB bandwidth fraction (BWF) or metric #2, to be maximized; and (3) the absolute difference between the frequency-averaged return elevation angle and 45 degrees (for normal incidence) or metric #3, to be minimized.

1.4. AMC Geometry Selection

A rectangular-patch metallic pattern was selected due to its simplicity, its ease of fabrication and suitability for use in ACAs, and the availability of LPM performance relations (which allow for full variation of the electromagnetic incidence angles for both polarizations) as well as HFM performance

results (within the literature). See Fig. 2. Therefore, it was decided that, due to a lack of available information in the literature and lack of time, that this single-band AMC pattern would be used instead of double-band patterns (as was originally intended).

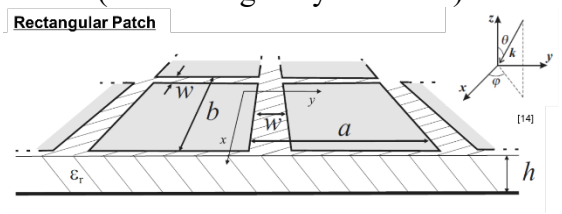

Figure 2: Selected AMC rectangular patch geometry.

2. AMC Model Development

The first step in assessing the ACA performance is to develop predictive capability for the ACA "building blocks" – the AMCs.

2.1. AMC LPM Development

The AMC impedance Z was determined using transmission line theory [14] as follows:

$$Z_i^{TM} = \frac{j\omega\mu_0\mu_r \frac{\tan(\beta h)}{\beta}\zeta}{1 - 2k_{eff}\alpha_{TM}\frac{\tan(\beta h)}{\beta}\zeta}$$

$$Z_i^{TE} = \frac{j\omega\mu_0\mu_r \frac{\tan(\beta h)}{\beta}}{1 - 2k_{eff}\alpha_{TE}\frac{\tan(\beta h)}{\beta}\xi}$$

where ω is the angular frequency,

$$\beta = \sqrt{k^2 - k_t^2}, k = k_0\sqrt{\varepsilon_r},$$

k_0 is the free-space wave number,

$$k_t = k_0 \sin\theta_0 \ [8],$$

$$k_{eff} = k_0\sqrt{\varepsilon_{eff}\mu_{eff}},$$

$$\varepsilon_{eff} = \frac{\varepsilon_r + 1}{2}, \quad \mu_{eff} = \frac{\mu_r + 1}{2},$$

$$\alpha_{TM} = \frac{k_{eff}a_{TM}}{\pi}\ln\left(\frac{1}{\sin\frac{\pi w}{2a_{TM}}}\right),$$

$$A_{TE} = \frac{k_{eff}a_{TE}}{\pi}\ln\left(\frac{1}{\sin\frac{\pi w}{2a_{TE}}}\right),$$

$$\theta_2 = \frac{\arcsin(\sin\theta_0)}{\sqrt{\varepsilon_r}}, \zeta = \cos^2\theta_2,$$

and $\xi = 1 - \frac{a_{TM}}{a_{TM}+a_{TE}}\left(\frac{k_0 \sin\theta_0}{k_{eff}}\right)^2$, with other parameters shown in Table 1.

Table 1. AMC parameters.

Frequency-Independent Input and Intermediate Data		
Type	**Parameter ***	**Units**
Inputs	Dielectric real relative permittivity $\varepsilon_{r'}$	-
	Dielectric loss tangent δ	
	Dielectric relative permittivity ε_r	
	Dielectric relative permeability μ_r	
	Free space permittivity ε_0	F/m
	Free space permeability μ_0	H/m
	Incidence elevation angle θ_0	deg
	Incidence azimuth angle ϕ_0	
	Dielectric thickness h	m
	Supercell periodicity d_{TM} within TM POI	
	Supercell periodicity d_{TE} within TE POI	
	AMC patch gap w	
	Minimum number of unit cells along TM POI	-
	Minimum number of unit cells along TE POI	
	RCSR goal	dB
Intermediates	AMC periodicity a_{TM} within TM POI	m
	AMC periodicity a_{TE} within TE POI	
	Free space impedance for TM polarization η_0^{TM}	Ω
	Free space impedance for TE polarization η_0^{TE}	
	Effective relative permittivity ε_{eff}	-
	Effective relative permeability μ_{eff}	
	Refraction angle θ_2	deg

* "TM" denotes transverse magnetic polarization, "TE" denotes transverse electric polarization, "POI" denotes plane of incidence

The supercell reflection phase P for AMC "i" and polarization "j" with respect to free-space impedance Z_0 can be expressed as

$$P_i^j = \mathrm{Im}\left[\ln\left(\frac{Z_i^j - Z_0^j}{Z_i^j + Z_0^j}\right)\right]$$

where for free space

$$Z_0^{TM} = \eta_0 \cos\theta_0$$

and

$$Z_0^{TE} = \frac{\eta_0}{\cos\theta_0}.$$

The supercell reflection amplitude A can be expressed as

$$A_i^j = \left|\frac{Z_i^j - Z_0^j}{Z_i^j + Z_0^j}\right|.$$

The supercell reflection loss RL (in dB) can be expressed as

$$RL_i^j = -20 \log A_i^j.$$

2.2. AMC HFM Development

A numerical, high-fidelity modeling (HFM) approach for simulating the AMC supercell was developed using the COMSOL 5.6 RF module [15]. This approach uses the finite element method to compute the amplitude and phase of reflected waves from electromagnetic structures. See Fig. 3 for the HFM representations.

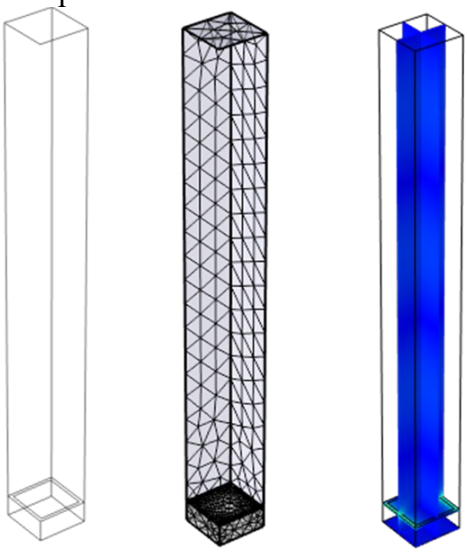

Figure 3: AMC HFM geometry, mesh, and predicted field cross-sections.

The Floquet port method in COMSOL 5.6 is employed for purposes of: (1) allowing simulation of a supercell by considering only a single unit cell; (2) correct accounting for phase shifts due to angle of incidence; and (3) simulation of spectral properties in terms of scattering (S) parameters; see Fig. 4.

Figure 4: Depiction of AMC HFM scattering parameter determination.

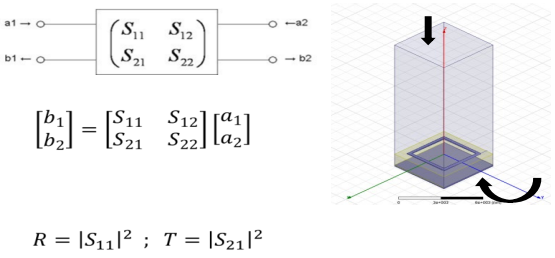

2.3. AMC LPM / HFM Validation

The previously discussed LPM and HFM models were used to simulate the performance of a square patch geometry scenario available from the literature [1], and compare the predicted and measured performance. Results associated with the reflection magnitude and phase can be seen in Figs. 5 and 6, respectively. Good agreement among the LPM, HFM, and literature results for the amplitude and phase characteristics of square patch reflection can be observed (in light of the different simulation methods and material property assumptions).

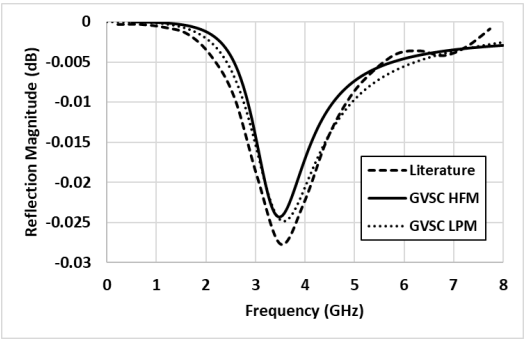

Figure 5: Predicted / measured AMC reflection magnitude.

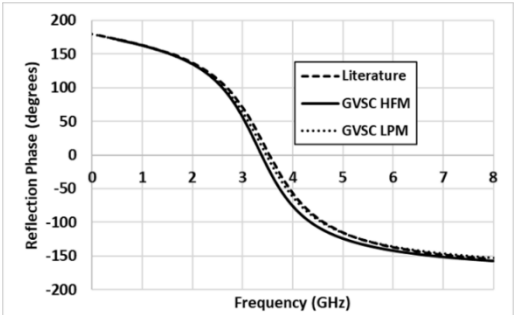

Figure 6: Predicted / measured AMC reflection phase.

3. ACA LPM Development

Up until now, the focus has been on the AMC model development. Now, we turn our attention to the ACA model development.

3.1. Scattered Lobe Direction And RCSR Predictive Capability

Using antenna planar array theory, the direction of the supercell scattering (grating) lobes can be approximately determined using the following expressions [12]:

$$\tan\phi_{m,n}^{j} = \frac{\sin\theta_0 \sin\phi_0 \pm (2n+1)\frac{\Delta P_{TM}^{j}}{kd_{TM}}}{\sin\theta_0 \cos\phi_0 \pm (2m+1)\frac{\Delta P_{TE}^{j}}{kd_{TE}}}$$

$$\sin^2\theta_{m,n}^{j} = \left[\sin\theta_0 \sin\phi_0 \pm (2n+1)\frac{\Delta P_{TM}^{j}}{kd_{TM}}\right]^2 + \left[\sin\theta_0 \cos\phi_0 \pm (2m+1)\frac{\Delta P_{TE}^{j}}{kd_{TE}}\right]^2$$

where q and f denote the elevation and azimuth angles with respect to the surface normal direction, 0 the incidence angles, DP the supercell phase shift, k the substrate wave number, d the supercell size, TE and TM the surface-tangential directions aligned with the TE and TM planes of incidence respectively, and m and n the reflection grating lobe order. The four major lobes can be determined by allowing m and n to equal zero [3].

A relation for ACA RCSR relative to a PEC is [1]:

$$\mathrm{RCSR} = 10\log\left[\frac{A_1 e^{jP_1} + A_2 e^{jP_2}}{2}\right]^2$$

where "A" denotes the reflection amplitude, "P" denotes the reflection phase, and the numeric subscript identifies the AMC supercell type.

3.2. Fresnel Coefficient Predictive Capability

The Fresnel reflection coefficient for transverse electrical polarization [5] is

$$R_{TE} = \frac{Z_i^{TE} - Z_0^{TE}}{Z_i^{TE} + Z_0^{TE}}$$

and for transverse magnetic polarization [5] is

$$R_{TM} = \frac{Z_i^{TM} - Z_0^{TM}}{Z_i^{TM} + Z_0^{TM}} .$$

While the relations for normal materials could generally be expressed for TE / TM polarization [5], the ground planes of these AMCs do not allow the development of an electric field and thereby prevent propagation of essentially any energy through the material. Therefore, for these AMCs, it can be effectively stated that the Fresnel transmission coefficients can be expressed as follows:

$$T_{TE} = 0$$

$$T_{TM} = 0 .$$

4. ACA LPM Optimization Study

Now that we've developed the ACA LPM, we can use it to perform optimization studies: a manual one and a DOE-based one. Both studies involved variation of the following parameters: (1) dielectric relative permittivity magnitude; (2) dielectric relative permittivity loss tangent; (3) dielectric thickness; (4) supercell periodicity (best results were obtained for equal periodicities along the TM and TE POIs); (5) patch gap for AMCs 1 and 2; and (6) the number of unit cells (per supercell). It was determined that minimizing the number of unit cells maximizes the scattering lobe elevation angles and azimuth angle standard deviations (both beneficial). However, it was also determined that the minimum number of unit cells which still allow supercell AMC

behavior to be obtained is four [10]. Therefore, four unit cells along both the TM and TE POIs were used. The scenarios considered involved an incident elevation angle of only 0 degrees, since the incident angle did not seem to be a significant discriminator of candidate performance. The previously discussed performance metrics were used.

4.1. Manual Optimization Study

The manual optimization approach involved "trial-and-error" selection of parameters in order to best improve the RCSR performance. The results of this study – which include the ACA LPM inputs and outputs – can be seen in Figs. 7 and 9.

4.2. DOE Optimization Study

To generate the DOE studies, Latin hypercube sampling was used to generate a large number of simulation cases which involved as wide a variation of the input parameters as possible. A MATLAB script was used for this purpose.

To execute the DOE studies, a Visual Basic script was used within the Excel-based LPM to solve several hundred thousands of cases. Multiple studies were performed, with the input parameter ranges becoming increasingly narrow, based upon the emerging results, for purposes of honing in on the best-performing case.

The results of this study – which include the ACA LPM inputs and outputs – can be seen in graphical form in Figs. 8 and 9, and in tabular form in Table 1. The DOE-optimized ACM pairing performs significantly better than the manually-optimized ACM pairing.

Frequency-Independent Input and Intermediate Data				
Type	Parameter *	Units	Value	
			AMC 1	AMC 2
Inputs	Dielectric real relative permittivity ε_r	-	2.2	
	Dielectric loss tangent δ		0.01	
	Dielectric relative permittivity ε_r		2.2+0.022000733362667i	
	Dielectric relative permeability μ_r		1	
	Free space permittivity ε_0	F/m	8.85419E-12	
	Free space permeability μ_0	H/m	1.25664E-06	
	Incidence elevation angle θ_0	deg	0	
	Incidence azimuth angle ϕ_0		0	
	Dielectric thickness h	m	0.0065	
	Supercell periodicity d_{TM} within TM POI		0.100	
	Supercell periodicity d_{TE} within TE POI		0.100	
	AMC patch gap w		0.0049	0.0224
	Minimum number of unit cells along TM POI	-	4	
	Minimum number of unit cells along TE POI		4	
	RCSR goal	dB	10	
Intermediates	AMC periodicity a_{TM} within TM POI	m	0.025	
	AMC periodicity a_{TE} within TE POI		0.025	
	Free space impedance for TM polarization η_0^{TM}	Ω	376.7	
	Free space impedance for TE polarization η_0^{TE}		376.7	
	Effective relative permittivity ε_{eff}	-	1.6-0.010003666833i	
	Effective relative permeability μ_{eff}		1	
	Refraction angle θ_2	deg	0.0	

* "TM" denotes transverse magnetic polarization, "TE" denotes transverse electric polarization, "POI" denotes plane of incidence

Output Data			
Type	Parameter *	Units	Value
Outputs **	Bandwidth fraction meeting RCSR goal for TM	%	43.1
	Bandwidth fraction meeting RCSR goal for TE		43.1
	RCS reduction for TM polarization	dB	8.56
	RCS reduction for TE polarization		8.56
	Scattering lobe elevation angle for TM	deg	15.5
	Scattering lobe elevation angle for TE		15.5
	Scattering lobe azimuth angle standard deviation for TM		45.0
	Scattering lobe azimuth angle standard deviation for TE		45.0

** Outputs are band-averaged with the exception of the bandwidth fractions

Figure 7: Manual optimization results

Frequency-Independent Input and Intermediate Data				
Type	Description *	Units	Value	
			AMC 1	AMC 2
Para-meters	Free space permittivity ε_0	F/m	8.85419E-12	
	Free space permeability μ_0	H/m	1.25664E-06	
Inputs	Dielectric relative permittivity magnitude ε_r	-	2.02E+00	
	Dielectric permittivity loss tangent δ		3.27E-02	
	Dielectric relative permeability μ_r		1	
	Incidence elevation angle θ_0	deg	0	
	Incidence azimuth angle ϕ_0		0	
	Dielectric thickness h	m	4.38E-03	
	Supercell periodicity d_{TM} within TM POI		0.063	
	Supercell periodicity d_{TE} within TE POI		0.063	
	AMC patch gap w		2.65E-03	1.36E-02
	Supercell periodicity along TM POI (super-cell / unit-cell periodicity)	-	4.0	
	Supercell periodicity along TE POI (super-cell / unit-cell periodicity)		4.0	
	Effective relative permeability μ_{eff}		1	
	RCSR goal	dB	10	
Intermediates	Unit cell periodicity a_{TM} within TM POI	m	1.57E-02	
	Unit cell periodicity a_{TE} within TE POI		1.57E-02	
	Free space impedance for TM polarization η_0^{TM}	Ω	376.7	
	Free space impedance for TE polarization η_0^{TE}		376.7	
	Dielectric relative permittivity ε_r	-	2.02053136167765-0.0660057786635422i	
	Effective relative permittivity ε_{eff}		1.5102688083883-0.0330028803177111i	
	Refraction angle θ_2	deg	0.0	

* "TM" denotes transverse magnetic polarization, "TE" denotes transverse electric polarization, "POI" denotes plane of incidence

Output Data			
Type	Description *	Units	Value
Outputs **	Bandwidth fraction meeting RCSR goal for TM	%	64.6
	Bandwidth fraction meeting RCSR goal for TE		64.6
	RCS reduction for TM polarization	dB	10.72
	RCS reduction for TE polarization		10.72
	Scattering lobe elevation angle delta for TM	deg	21.2
	Scattering lobe elevation angle delta for TE		21.2
	Scattering lobe azimuth angle standard deviation for TM		45.0
	Scattering lobe azimuth angle standard deviation for TE		45.0

** Outputs are band-averaged with the exception of the bandwidth fractions

Figure 8: DOE optimization results

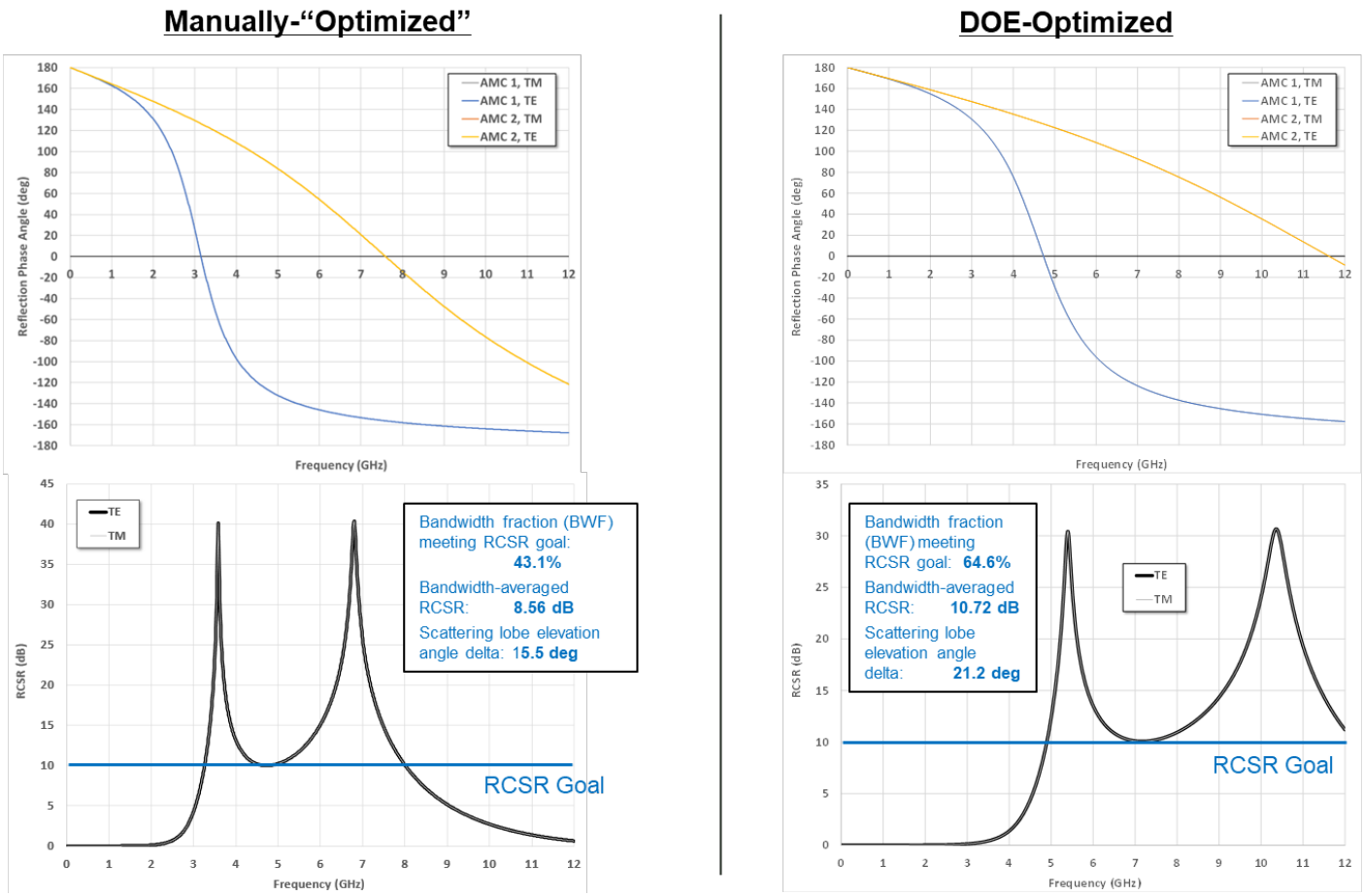

Figure 9: Manual and DOE optimization result comparison

Output Comparison			
Metric	Value		Units
	Manually-Optimized	DOE-Optimized	
Bandwidth fraction meeting RCSR goal	43.1	64.6	%
Bandwidth-averaged RCSR	8.6	10.7	dB
Scattering lobe elevation angle delta	15.5	21.2	deg

Table 1: Manual and DOE optimization result comparison

5. ACA MFM Simulation

What's ultimately needed is ACA performance predictive capability which can accommodate realistic vehicle integration geometries. A review of the ACA predictive capability developed so far reveals that the LPM only accommodates simple, flat-plate scenarios, and that the HFM cannot accommodate complex geometries due to its solving of the full Maxwell equations. To fill this gap, it would be desirable to develop "in-between" (or MFM) predictive capability, which would involve the solution of the governing Maxwell equations as simplified for the optical regime using the Xpatch computational electromagnetics asymptotic solver.

5.1. ACA MFM Methodology

Xpatch uses the shooting and bouncing ray (SBR) tracing method, combining geometric and physical optics methods. Diffraction effects are modeled based upon the physical theory of diffraction. Material discontinuities and both co- and cross-polarizations are accounted for.

The MFM would be used to model the ACAs and predict the interactions of the checkerboard-patterned AMC supercells.

The MFM is developed based upon the following considerations / assumptions.

- The AMC supercells can be modeled using Fresnel reflection and transmission coefficients. These coefficients – involving both the real and imaginary components for both the TE and TM polarizations – were determined for the DOE-optimized AMC supercell combination over the full range of frequencies and incidence angles using a Visual Basic script.
- The MFM approach can be used to assess the ACA RCSR performance both for simple plates and notional ACA-integrated vehicles.

5.2. ACA MFM Plate Study

Using the MFM, a simple flat plate analysis was performed for purposes of comparing a "bare plate" and an "ACA-treated plate"; see Fig. 10. "AMC 1" is shown in red color, while "AMC 2" is shown in blue color.

The angle of incidence is assumed to vary only in the azimuth (and not elevation) direction. For purposes of simplicity, the results associated with only the two co-polarizations – vertical receive / transmit (VV) and horizontal receive / transmit (HH) – are considered. The rationale for this limitation involves the fact that co-polarization returns are generally more significant than cross-polarization returns. It should also be noted that the VV polarization results are associated with the TE-polarization AMC behavior, and the HH polarization results are associated with the TM-polarization AMC behavior.

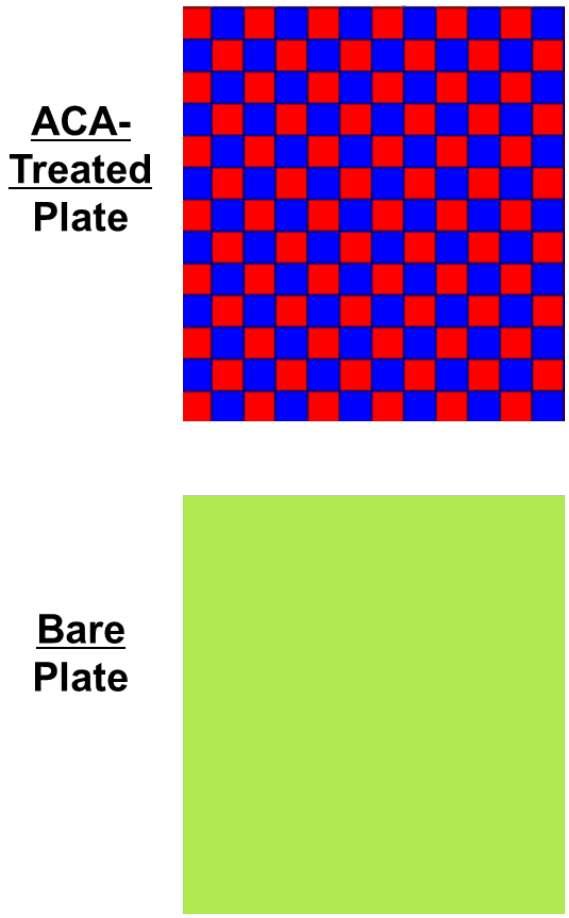

Figure 10: ACA-treated and bare plate

The results associated with this study can be seen in tabulated form in Table 2, and in graphical form in Fig. 11. The MFM plate study results – including both the predicted RCSR and the bandwidth fraction (BWF) over which the RCSR goal is met – compare relatively favorably with the LPM results, especially at normal (zero degrees) incidence angle, which is the most important incidence angle as it relates to RCSR. Based upon this positive MFM validation exercise (for a flat plate), it was then desired to perform further studies (which are not presented here).

Table 2: ACA MFM plate study results

RCSR

VV

Incidence Azimuth Angle (deg)	RCS (dB) for VV Polarization and Various Bandwidths					
	MFM-Predicted					LPM-Predicted
	L-Band (1-2 GHz)	S-Band (2-4 GHz)	C-Band (4-8 GHz)	X-Band (8-12 GHz)	Band-Averaged (1-12 GHz)	
0	0.0	0.3	11.6	19.0	11.2	10.7
15	0.0	0.2	6.2	18.2	8.9	10.4
30	0.0	0.1	9.3	15.2	8.9	9.2
45	0.0	0.1	5.8	8.2	5.1	6.2
60	0.0	0.0	4.7	3.6	3.0	3.5
75	0.0	0.0	2.5	1.0	1.3	1.4
89	0.0	0.0	0.1	0.0	0.0	0.1

BWF

VV

Incidence Azimuth Angle (deg)	Bandwidth Fraction Over Which RCSR Goal Is Met for VV Polarization and Various Bandwidths					
	MFM-Predicted					LPM-Predicted
	L-Band (1-2 GHz)	S-Band (2-4 GHz)	C-Band (4-8 GHz)	X-Band (8-12 GHz)	Band-Averaged (1-12 GHz)	
0	0.000	0.000	0.777	1.000	0.646	0.646
15	0.000	0.000	0.223	0.969	0.433	0.530
30	0.000	0.000	0.316	0.699	0.369	0.383
45	0.000	0.000	0.133	0.328	0.168	0.204
60	0.000	0.000	0.137	0.000	0.050	0.054
75	0.000	0.000	0.070	0.000	0.026	0.026
89	0.000	0.000	0.000	0.000	0.000	0.000

HH

Incidence Azimuth Angle (deg)	RCS (dB) for HH Polarization and Various Bandwidths					
	MFM-Predicted					LPM-Predicted
	L-Band (1-2 GHz)	S-Band (2-4 GHz)	C-Band (4-8 GHz)	X-Band (8-12 GHz)	Band-Averaged (1-12 GHz)	
0	0.0	0.3	11.6	19.0	11.2	10.7
15	0.0	0.2	6.8	18.9	9.4	11.0
30	0.0	0.1	12.2	18.4	11.1	12.0
45	0.0	0.2	12.8	19.3	11.7	14.5
60	0.0	0.2	5.1	12.5	6.5	7.8
75	0.0	0.1	1.4	4.0	2.0	2.3
89	0.0	0.0	-0.1	-0.1	-0.1	0.0

HH

Incidence Azimuth Angle (deg)	Bandwidth Fraction Over Which RCSR Goal Is Met for HH Polarization and Various Bandwidths					
	MFM-Predicted					LPM-Predicted
	L-Band (1-2 GHz)	S-Band (2-4 GHz)	C-Band (4-8 GHz)	X-Band (8-12 GHz)	Band-Averaged (1-12 GHz)	
0	0.000	0.000	0.777	1.000	0.646	0.646
15	0.000	0.000	0.469	0.973	0.524	0.639
30	0.000	0.000	0.648	0.855	0.547	0.620
45	0.000	0.000	0.496	0.863	0.494	0.581
60	0.000	0.000	0.188	0.855	0.379	0.463
75	0.000	0.000	0.000	0.000	0.000	0.000
89	0.000	0.000	0.000	0.000	0.000	0.000

Figure 11: ACA MFM plate study results

6. Genetic Programming Investigations

For purposes of improving performance through more thorough investigation of the ACA design space, GP books, papers, webpages, and codes were investigated. For FY24, the HeuristicLab software was tentatively selected for use in evolving candidate AMCs based upon past candidate electromagnetic (EM) performance trends. The parameters to be varied would include dielectric permittivity, substrate thickness, and the metallic patch topology. The topology would be varied by the addition / subtraction of material in the shape of a circle of specified radius and position.

It is planned to use COMSOL to generate AMC candidate geometry based upon HeuristicLab output, as well as perform RF EM analyses to characterize candidate AMC reflection magnitude and phase over the desired range of frequencies. It is also planned to continue using the already-developed Excel-based ACA solver, and to further develop it to use the COMSOL-outputted ACA candidate performance data. A flowchart depicting the entire planned, automated, GP-based geometry creation, analysis, and evolution process is shown in Fig. 12.

7. Summary and Conclusions

It was desired to develop a thin ACA metasurface concept which could be constructed and adhered to materiel surfaces for purposes of reducing their radar cross section. A rectangular-patch metallic pattern was selected due to its simplicity, ease of fabrication, and availability of both LPM performance relations and HFM performance results in the literature for validation purposes. The lack of consideration of other topologies limited RCSR performance potential. A set of optimization goals was developed for the purpose of having a means by which to compare the developed concepts.

AMC LPMs and HFMs were successfully developed and validated using experimental data from the literature, and ACA LPMs and MFMs were successfully developed and correlated. Using the ACA LPM, the DOE-optimized ACM pairing was found to perform significantly better than the manually-optimized ACM pairing.

The MFM plate study RCSR and BWF results compared relatively favorably with the LPM results, especially at normal (zero degrees) incidence angle, which is the most important incidence angle as it relates to RCSR. Additional integration studies were performed, and may be presented in the future.

GP approaches, methodologies, and tools were researched and considered, and a GP-based plan for follow-on efforts was established at a high level. Such a plan would ideally be executed first for two-dimensional ACMs (second year) and then for three-dimensional ACMs (third year, potentially).

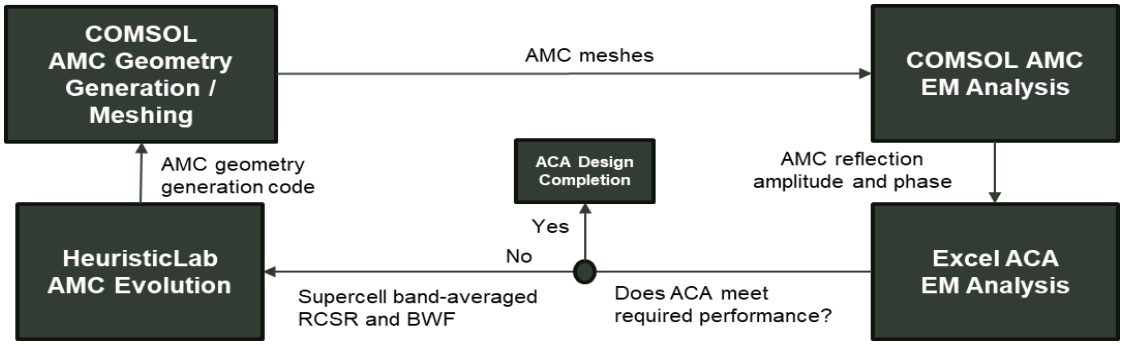

Figure 12: GP-based geometry creation, analysis, and evolution

8. REFERENCES

[1] Chen, Wengang, Constantine A. Balanis, and Craig R. Birtcher. "Checkerboard EBG surfaces for wideband radar cross section reduction." IEEE Transactions on Antennas and Propagation 63.6 (2015): 2636-2645.

[2] Rayno, Jennifer H. Development and application of genetic programming in the design and optimization of ultra-wideband 3D metamaterials. Diss. Univ. of Hawai'i at Manoa, 2016.

[3] Balanis, Constantine A., et al. "Applications of AMC-based impedance surfaces." EPJ Applied Metamaterials 5 (2018): 3.

[4]Sievenpiper, Daniel Frederic. High-impedance electromagnetic surfaces. University of California, Los Angeles, 1999.

[5] Balanis, Constantine A. Advanced engineering electromagnetics. John Wiley & Sons, 2012.

[6] Luukkonen, Olli, et al. "Simple and accurate analytical model of planar grids and high-impedance surfaces comprising metal strips or patches." IEEE Transactions on Antennas and Propagation 56.6 (2008): 1624-1632.

[7] Xu, Yuan, and Mang He. "Design of multilayer frequency-selective surfaces by equivalent circuit method and basic building blocks." International Journal of Antennas and propagation 2019 (2019).

[8] Costa, Filippo, Agostino Monorchio, and Giuliano Manara. "An overview of equivalent circuit modeling techniques of frequency selective surfaces and metasurfaces." The Applied Computational Electromagnetics Society Journal (ACES) (2014): 960-976.

[9] Hosseinipanah, Mirshahram, and Qun Wu. "Equivalent circuit model for designing of Jerusalem cross-based artificial magnetic conductors." Radioengineering 18.4 (2009): 544-550.

[10] Galarregui, Juan Carlos Iriarte, et al. "Broadband radar cross-section reduction using AMC technology." IEEE Transactions on Antennas and Propagation 61.12 (2013): 6136-6143.

[11] Durgun, Ahmet Cemal. Analysis, Design, Simulation, and Measurements of Flexible High Impedance Surfaces. Arizona State University, 2013.

[12] Balanis, Constantine A., et al. "Applications of AMC-based impedance surfaces." EPJ Applied Metamaterials 5 (2018): 3.

[13] Sang, Di, et al. "Design of checkerboard AMC structure for wideband RCS reduction." IEEE Transactions on Antennas and Propagation 67.4 (2019): 2604-2612.

[14] O. Luukkonen, “Artificial impedance surfaces,” Ph.D. Dissertation, Department of Radio Science and Engineering,

Helsinki University of Technology, Espoo, Finland, 2009.

[15] COMSOL v. 5.6 RF module user manual.